

Microlensing path parametrization for Earth-like Exoplanet detection around solar mass stars

L. DE ALMEIDA¹ AND J.-D. DO NASCIMENTO JR.^{1,2,3}

¹*Dep. de Física, Univ. Federal do Rio Grande do Norte
59072-970 Natal, RN, Brazil*

²*Harvard-Smithsonian Center for Astrophysics
60 Garden St., Cambridge, MA 02138, USA*

³*Universit Paris-Sud, CNRS, Institut d'Astrophysique
Spatiale, UMR 8617, 91405, Orsay Cedex, France*

(Received ...; Revised ...; Accepted ...)

ABSTRACT

We propose a new parametrization of the impact parameter u_0 and impact angle α for microlensing systems composed by an Earth-like Exoplanet around a Solar mass Star at 1 AU. We present the caustic topology of such system, as well as the related light curves generated by using such a new parametrization. Based on the same density of points and accuracy of regular methods, we obtain results 5 times faster for discovering Earth-like exoplanet. In this big data revolution of photometric astronomy, our method will impact future missions like WFIRST (NASA) and Euclid (ESA) and they data pipelines, providing a rapid and deep detection of exoplanets for this specific class of microlensing event that might otherwise be lost.

Keywords: microlensing technique, exoplanets, close topology, path parametrization

1. INTRODUCTION

Gravitational lensing of a point source creates two images with combined brightness exceeding that of the source. For small separation between the two images the only observable consequence of the lensing is an apparent source brightness variation. This phenomenon is referred as gravitational microlensing (Einstein 1936; Liebes 1964; Paczynski 1986; Mao & Paczynski 1991). Gravitational microlensing, among other things, is used as a constraint for several questions in astrophysics and cosmology, as for example to study primordial black holes (Griest et al. 2011) and galaxy dark matter halo Alcock et al. (1995). Simultaneously, the study of exoplanets has grown since the discovery of the first exoplanet orbiting a sun-like star (Mayor & Queloz 1995) and among several branches the study of habitability (Beaulieu et al. 2011; do Nascimento et al. 2016) has become one of the most active stellar astrophysics subjects. Currently, a new surprisingly successful application concerning microlensing is its capability to finding furthest and smallest planets outside the snow line re-

gion as compared to any available extrasolar planets detection method (Gould & Loeb 1992; Bennett & Rhie 1996). The gravitational microlensing detections made so far present a variety of binary systems, and the detection sensitivity for semimajor axis ranges from 0.5 AU to 10 AU and the medium mass of the host star is $0.35M_{\odot}$ (Cassan et al. 2012). For these systems, the mass ratio, q , between the planet (m_2) and host star (m_1), $q = m_2/m_1$ is higher than 1×10^{-4} . to date eight microlensing planets with planet-hot mass ratio $q < 1 \times 10^{-4}$ have been characterized (Udalski et al. 2018). Gravitational microlensing is directly sensitive to the ratio of the masses of the planets and its host star, and the light curve give us the projected apparent **semimajor** axis for the system normalized to the Einstein radius.

From the observational side, the surveys Microlensing Planet Search (MPS) (Rhie 1999) and Microlensing Observations in Astrophysics (MOA) (Rhie et al. 2000; Sumi et al. 2003) demonstrated for the first time that microlensing technique is sensitive enough to detect earth-mass exoplanets.

Shvartzvald et al. (2017) show the possibility to detect Earth-mass Planet in a 1 AU Orbit around an Ultracool

Dwarf and Yee et al. (2009) present an extreme magnification microlensing event and its sensitivity to planets with masses as small as $0.2M_{\oplus} \simeq 2M_{Mars}$ with projected separations near the Einstein ring (3 AU). Gould et al. (2014) even showed the capability of microlensing technique to discover Earth-mass planets around 1 AU in binary systems. As discussed by Albrow et al. (2001); Gaudi et al. (2002), more than 77% of exoplanetary systems discovered with microlensing techniques shows planets with masses lower than Jupiter mass and with **semimajor** axis between 1.5 and 4 AU. These results are consistent with the fact that massive planets far away from their central stars are easier to be detected with microlensing method (Sumi et al 2006; Han 2006). In this context, Paczynski (1986) shows that detection is function of the impact parameter u_0 and the impact angle α . Here, in this study we propose a parametrization of the source's path to force it to cross the Caustic Region Of INterest (CROIN by Penny 2014). This offers an advantage for detecting Earth-like planets around Solar-like stars during microlensing events.

In Section 2 we describe the lens equation and the semi-analytic method. We explore the caustic topology for events with a **semimajor** axis of about 1 AU, with the lens at 7.86 kpc and source at 8 kpc in Section 3 and explore the close systems topology geometry in Section 3.1 as well describe our parametrization proposal. We present light curves where it is possible to conduct an analysis of the u_0 and α variation as a function of a fixed parameters in the lens-planet apparent separation in Section 3.2. We constructed a model to simulate our system based on a semi-analytical method for solving the binary lens equation to take into account the source, lenses, caustic, critic curves and producing images and light curves. We present the resume of our simulations and discussion of our results in Section 4.

2. THE LENS EQUATION

A gravitational microlensing event occurs when a star in the foreground (lens) passes near the line of sight of a background star (source) and **thereby bends the source light** from the original path. This bending of the light generates a relative magnification of the source and if the system source-lens have relative movements, a characteristic light curve is produced. The deflection of the light by a single star can be **expressed** by $\alpha = \frac{4GM}{c^2 r}$, where α is the deflection angle, M the lens mass, G is the universal gravitational constant, c is the speed of light and r is the **impact parameter**. If we establish D_S as the distance between the observer and the source and D_L as the distance between the observer and the lens, we can write the distance between the source and

lens as $(D_S - D_L)$, and we can derive the **well known** equation of the Einstein Radius

$$\theta_E = \sqrt{\frac{4GM}{c^2} \frac{D_S - D_L}{D_L D_S}}. \quad (1)$$

The equation 1 holds regardless on the alignment between the source and the lens, but if they are aligned, we have the so called Einstein ring. Introducing the small distance β between the source and the lens, we can derive the lens equation for the single lens case as $\beta = \theta - \frac{\theta_E^2}{\theta}$ which is the well known lens equation for the single lens case, and it can be easily solved as a second degree polynomial.

2.1. Formalism

For the binary-lens case, we can rewrite β , originally written for single lens case, using the complex notation to denote the lens equation for the two lenses (Witt H. J 1990; Witt & Mao 1995) case, representing a host star and their planet as

$$\omega = z - \frac{\varepsilon_1}{\bar{z} + \bar{z}_1} - \frac{\varepsilon_2}{\bar{z} + \bar{z}_2}. \quad (2)$$

In the above equation, ε_1 and ε_2 are the normalized lenses masses, with $\varepsilon_1 + \varepsilon_2 = 1$. The parameter z is the **two-dimensional position written as the real and imaginary components of a complex number**. The ω is the relative position of the source at a specific time. **The bar over complex quantities indicates complex conjugation.**

2.2. The semi-analytic method

Technically, to solve a lens equation with $n = 2$, it is necessary to invert a 5th order polynomial and solve it to find the polynomial roots. To accomplish this task we developed a model that uses a semi-analytic method to find polynomial coefficients and solutions (Witt H. J 1990). For the case where the source is not close enough to the caustic-crossing region, we used the point source magnification method to solve and obtain the light curve.

3. EARTH-MASS LIKE SYSTEMS TOPOLOGY

Caustics modeling and microlensing critical event curves depends fundamentally on the apparent **semimajor** axis s between the lenses, i.e., the host lens and the planet. Here we used Einstein radius units R_E , and the mass fraction as $q = m_2/m_1$, **where m_2 stands for the planet mass and m_1 mass of the star**. The source's path is defined by 2 parameters, the impact parameter u_0 and the impact angle α . The impact parameter u_0 represents the closest distance between the source and the host lens at the time t_0 .

In general, binary systems caustics produce **close, resonant, and wide topologies** (Schneider & Weiss 1987; Erdl & Schneider 1993), and with limits varying as a function of s and q . For this case, the impact angle α is the angle between the source trajectory and the x -axis of to the system. For the **binary-lens** case, the system lies in the x -axis.

For systems like our Sun-Earth system, in terms of Earth-Sun mass ratio, we find $q = 3 \times 10^{-6}$ and $s = 0.95969$, whereas the $m_1 = M_\odot$, $m_2 = M_\oplus$ and $1R_E = 1.0420$ AU. In such a system, a planet orbiting a **semimajor** axis of 1 AU **would lie** at the Einstein Ring limit. Nevertheless, we can not ignore possible values of $s < 1$ AU due to the fact that for **this system** the **semimajor** axis is the projected separation between the planet and its host star. By considering systems with $q = 3 \times 10^{-6}$ and s as a **free positive parameter**, two topologies **are more likely to** be obtained, wide or close. As presented by (Erdl & Schneider 1993), systems with such a wide topology satisfy the condition

$$s > \sqrt{\frac{(1 + q^{\frac{1}{3}})^3}{1 + q}}. \quad (3)$$

For the interval $0.1 < s < 0.95969$, our system can only be close. Thus, to adjust the u_0 and α parameters in an efficient way, we need to know the position of the planetary caustic as a function of the s variation.

By analyzing equation 3, we can conclude that a system with an Earth-Sun mass ratio can only be within a wide topology if $s > 1.0217R_E$. On the other hand, as our system can only assume $0.1R_E < s < 0.95969$, we can discard the wide topology for systems like our own. Thus, to use microlensing path parametrization for Earth-like exoplanet detections around solar mass stars, a deep analysis of the close topology case is necessary.

3.1. close topology case

The close topology is formed by three caustics. A central caustic close to the primary lens and two identical planetary caustics **on either side of the system axis** and opposite side of the planet. For a light curve of a source that passes close the central caustic and on the same side as the planet, we are able to detect only the main lens signature. Following results by Erdl & Schneider (1993), we can define a such close topology system when the condition below is satisfied

$$\frac{q}{(1+q)^2} < s^{-8} \left(\frac{1-s^4}{3} \right)^3. \quad (4)$$

In the above equation, for $q = 3 \times 10^{-6}$, a system like our Sun-Earth system can only be close if $s < 0.9893$. In

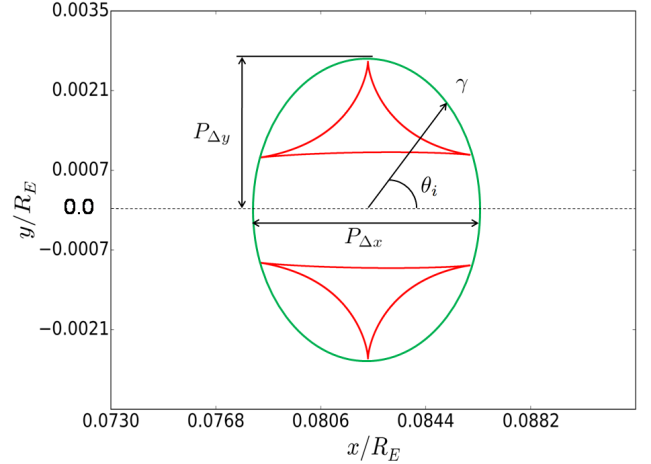


Figure 1. Planetary caustic in detail with $q = 3.003467 \times 10^{-6}$, $s = 0.9597E_R$, $u_0 = 0.0082E_R$. The green ellipse is the influence area **defined** by the equation 10

order to set the region of influence, we need at this point, to define the planetary caustic characteristics for close systems. Considering x as the position of the planetary caustic, that can be determined through the following equation (Han 2006)

$$X_{pc} = \frac{1}{1+q} \left(s - \frac{1-q}{s} \right), \quad (5)$$

where X_{pc} is the the separation **between the primary** lens and the center of the planetary caustic. The equation 5 makes clear that the smaller s , the larger the value of X_{pc} . By using this position X_{pc} we were able to parametrized some geometrical proprieties of the system and also to set the dependency of the source's path with the localization of the influence region around the planetary caustic. We can also link the position X_{pc} of the planetary caustic center with the impact parameter u_0 by the following equation

$$u_0 = \frac{|s^2 + q - 1| \cdot |\tan(\alpha)|}{|q + 1| \cdot |s| \cdot \sqrt{\tan(\alpha)^2 + 1}}. \quad (6)$$

To better describe the entire region of interest we need to geometrically describe the entire area containing the planetary caustic. For that, following the geometry of the problem, we found values for $P_{\Delta x}$ and $P_{\Delta y}$, (Figure 1) written below

$$P_{\Delta x} = \frac{3}{2} s^3 \sqrt{3} \sqrt{q}, \quad (7)$$

$$P_{\Delta y} = 2 \frac{\sqrt{q}}{s \sqrt{s^2 + 1}}. \quad (8)$$

For close topologies in this regime, the planetary caustic can be enclosed by an ellipse independent of its size.

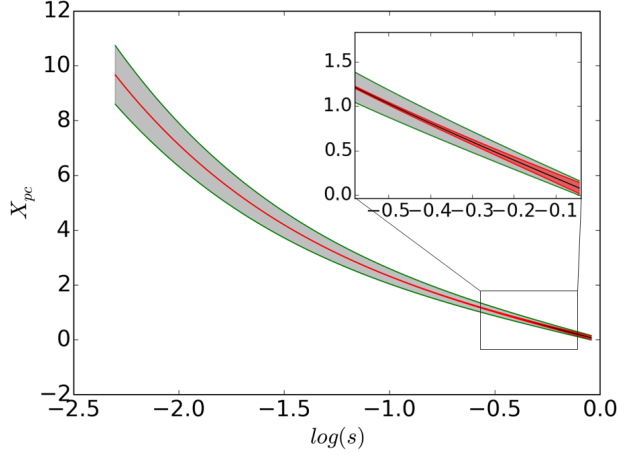


Figure 2. X_{pc} as a function of $\log s$ for our **adopted** system with $q = 3.003467 \times 10^{-6}$ and $0.95969 > s > 0.1$. The gray region is $2P_{\Delta y}$ and the red region is $P_{\Delta x}$ (both multiplied by twenty for better visualization)

Thus the size of the influence area, which contains the planetary caustic, can be defined through an ellipse area πab , with $a = P_{\Delta x}/2$ and $b = P_{\Delta y}$. Thus, the influence area that define the region containing the planetary caustic is

$$A = \pi \frac{P_{\Delta x}}{2} P_{\Delta y}. \quad (9)$$

Entering the equations 7 and 8 into the equation 9, we determined the **area** A that contains the planetary caustic as presented by the green ellipse in the figure 1, and now as a function of q and s

$$A = \frac{\gamma^2 \pi s^2 \sqrt{3q}}{\sqrt{s^2 + 1}}, \quad (10)$$

where γ is a scalar factor for the size of the area which contains the planetary caustic. For the particular case of γ equal to 1, figure 1, such area fits perfectly the planetary caustic.

By analyzing figure 2 we find that, for systems with close topology, the distance X_{pc} increases as s decreases. We can also see, based on equations 7 and 8, that $P_{\Delta x}$ drastically decreases and $P_{\Delta y}$ increase when s approaches the origin. Equation 10 leads to the conclusion that the area of the planetary caustic overall decreases when s approaches to origin. Thus, even with X_{pc} getting bigger when s decreases, the total area is not enough for any possible detection. Figure 2 leads to the conclusion that $2P_{\Delta y}$ and $P_{\Delta x}$ approaches to same value when s approaches to 1.

To link the source path with the *Caustic Region Of Influence* (CROIN) as described by Penny (2014), we

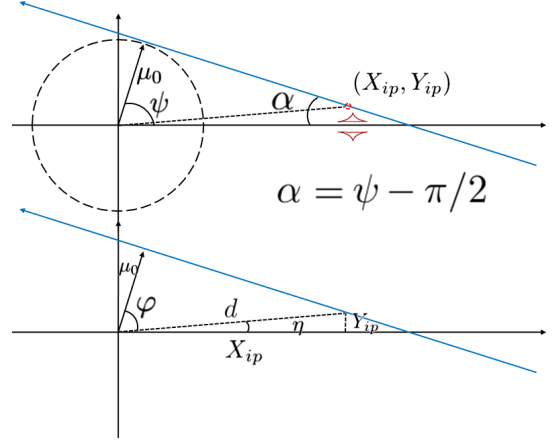


Figure 3. Top panel: Topology of a close system showing the point of interest from equations 18 and 19. Bottom panel: the geometry of the system with relative angles.

define all the points on the ellipse using the equations 7 and 8 as

$$X_{ip} = \gamma P_{\Delta x} \cos(\theta_i) + X_{pc}, \quad (11)$$

$$Y_{ip} = \gamma P_{\Delta y} \sin(\theta_i). \quad (12)$$

If we evolve θ_i from 0 to 2π in the equations above, we define the perimeter of the ellipse of area A , for the close topology case. Now, we can define the parameterization of the source path to the close topology case by the next equation

$$u_i = \frac{|\tan(\alpha) X_{ip} - Y_{ip}|}{\sqrt{\tan(\alpha)^2 + 1}}. \quad (13)$$

By setting $\gamma = 1$, and varying α from 0 to 2π , we **obtain all** values of u_0 from the equation 13 with the path of the source always passing by the planetary caustic vicinity. Thus, to explore all the possible light curves for our Earth-Sun model, we need to vary γ , α and θ_i . Furthermore we know from (Paczynski 1986) that, when analysing a microlensing event, the parameters t_E , t_0 and u_0 are the firsts to be **established** from the single-lens model. It is more interesting here to parametrize α in respect to u_0 , because the impact parameter u_0 is already set to a small error from the single-lens model. We can note that the equation 13 is impossible to be inverted in terms of $\alpha(u_0)$, so we need to find another method to express the parametrization of α in respect to u_0 .

To achieve that we need to find a function $\alpha(u_0)$ which depends only on the position of interest given by X_{ip} and Y_{ip} , and the impact parameter u_0 . By analysing the geometry (figure 3), we get $d = (X_{ip}^2 + Y_{ip}^2)^{1/2}$, $\eta =$

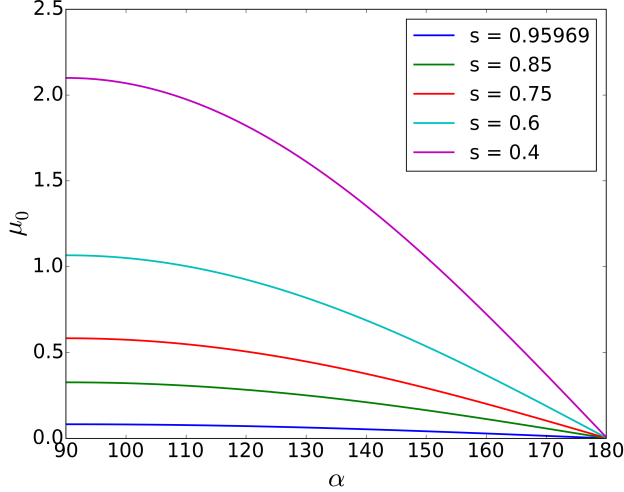


Figure 4. Evolution of the impact angle α when different initial mu_0 is set for $s = 0.95969, 0.85, 0.75, 0.6$ e 0.4 .

$acos(X_{ip}/d)$ and $\varphi = acos(u_0/d)$. The impact angle α is $\psi - \pi/2$ with ψ being the sum of η and φ . Then, we can simplify our new function α as:

$$\alpha(u_0) = acos\left(\frac{u_0}{\sqrt{X_{ip}^2 + Y_{ip}^2}}\right) - asin\left(\frac{X_{ip}}{\sqrt{X_{ip}^2 + Y_{ip}^2}}\right). \quad (14)$$

Notice that equation 14 depends solely on q , s and u_0 and can fill the area of the planetary caustic by varying γ . This parametrization **only covers** the set of q and s that generate close topologies. For values out of this range (wide or resonant), we can not use this parametrization. The evolution of the impact angle α was computed when different initial u_0 was set as $s = 0.95969, 0.85, 0.75, 0.6$ and 0.4 . For all cases the impact parameter u_0 must be smaller than the position of the planetary caustic or else the path of the source will not pass through the region of influence.

Figure 4 presents the evolution of the impact angle α when different initial u_0 is set to $s = 0.95969, 0.85, 0.75, 0.6$ and 0.4 . We can see in all cases that the impact parameter u_0 must be smaller than the position of the planetary caustic or else the path of the source will not pass through the region of influence.

From the figure 4 and relative equation 6 we see that, as α approaches 90° (perpendicular with the lens axis) the value of u_0 increases. That happens because, in order to the source's path to cross the interest region in X_{pc} , u_0 **needs to** be 0 so that $\alpha = 2\pi$ and if the path is perpendicular, with $\alpha = \pi/2$, than u_0 must be set to

the value of X_{pc} . According to Penny (2014), this kind of parametrization can greatly accelerate the simulation of light curves in the search for low-mass planets, but at the cost of passing by possible detections in unlikely topologies.

3.2. Light curves for close systems

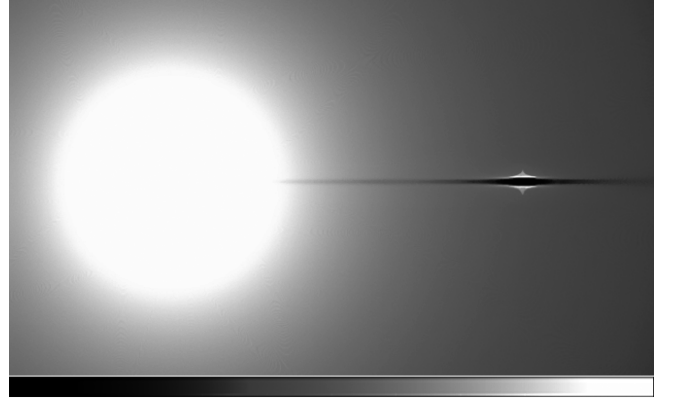


Figure 5. Magnification map of a system with $q = 3.003467 \times 10^{-6}$ and $s = 0.9597E_R$. The color bar shows arbitrary values from low magnification (black) to high magnification (white).

Once we have the parametrization of $\alpha(u_0)$ and $u_0(\alpha)$ in respect to the positions X_{ip} and Y_{ip} , we can generate all the light curves within the region of interest by varying γ in the equations 11 e 12. Figure 6 shows a light curve of a system that mimics our own Sun-Earth system with $q = 3.003467 \times 10^{-6}$, $s = 0.95969$ and path parameters as $u_0 = 0.15$, and $\alpha = 0.587$. We note a negative magnification at the planetary crossing region due to the source passing between the two planetary caustics. This negative magnification can be better visualized in the figure 5.

Figure 5 shows the magnification map of our system created by using a 5000×5000 pixels grid with arbitrary values for magnification. We can see that the central lens is responsible for almost all magnification of the source. The deviation due to the planetary caustic is negative between the two caustics but **also presents** a positive magnification at the crossing caustic regions.

By using the equation 14 we generated several light curves by setting a fixed value for $u_0 = 0.15$ and varying γ from -4 to 10 thus, evolving the values of α from 0.422 (black line) to 0.853 (blue line). From our parametrization, we can see in the figure 6 **that the**

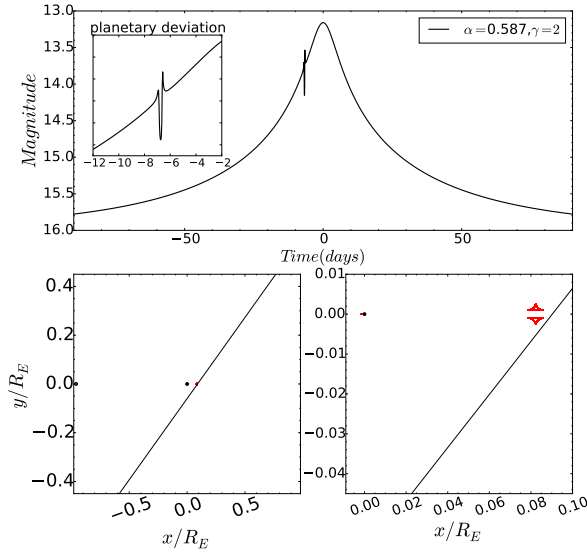


Figure 6. Top panel: light curve model for Sun-Earth system with $q = 3.003467 \times 10^{-6}$ and $s = 0.95969$ with a close-up at the planetary deviation. Bottom panel: left panel shows a wide view of the system with the path in blue; right panel is a close-up of the planetary caustic.

overall aspect of the light curve for a single-lens case is preserved and that the end of all possible planetary deviations are superposing the same line. Thus, given the initial parameters t_0 , t_E and u_0 from a single-lens approximation scenario we are able to generate all possible light curves that could present a detectable planetary deviation. The detection itself depends on the observational cadence.

To demonstrate the computational efficiency and an increase of the precision from our method we performed a computational experiment and produced synthetic systems with the following parameters:

- *cadence*: 24 daily photometric measurements
- *tobserv*: observational duration: 90 days
- *number of points*: cadence*tobserv
- *u*: impact parameter = 0.05
- *alpha*: inclination of impact = -2.489
- *q*: mass fraction = 3.003467e-6
- *s*: **normalized projected separation** = -0.95969
- *tE*: time in days to cross the Einstein radius = tobserv / 2

The experiment **generates** synthetic data with 4320 photometric points spread along 90 days and with a record every 1 hour. We apply a Gaussian noise error of 0.5% in the photometric measurement.

Based on the synthetic light curves, a systematic search for parameters was performed by setting q and s as our simulated system. Then, the same systematic search for parameters was performed by using our new parameterization. On the conventional method, we need to cover the dispersion of the q and s parameters, and we need also to cover the impact angle variation as $2\pi > \alpha > 0$. We set all other parameters as described above and a search now only on the α . The denser variation of α **gives more** accuracy to the result. We run the code to cover $2\pi > \alpha > 0$ with 1000 points. After that, we run the code using our model, varying the parameter γ from -5 to 8 , with the same points quantity. We show in the figure 8 the comparative performance result between our method and the conventional one. From the figure 8 the blue line represents the search process by using our model. We can see that, the search performed with the conventional model (black line) **covers** some unnecessary regions of the **alpha domain**. A second aspect is that in addition to **region covered**, we have less resolution in the regions of smaller χ^2 . We see that α and u_0 parameterization with respect to CROIN, forces the search to be focused only in the region that it would be possible to detect our kind of interested system.

As far as the parameterization deals with a focused search process, its efficiency is mainly controlled by the ratio between the global search α (conventional model) and the focused one γ . Based on that, we conclude that, for this particular case, we arrive at the same result with a precision rate 5.2 higher, and by using 1000 points in a range of 0.6 rad, instead π on the conventional one. For the same density of points and accuracy, **our methods is 5 times faster to converge to the best fit and this is one of advantages.**

4. SUMMARY AND DISCUSSION

We analyzed a set of simulations constructed to search Earth-like exoplanet around solar mass stars. Our simulations involved a parameter search on Sun-Earth models created using the semi-analytical method. We find that all solutions involving close topologies are not degenerated and since we are searching only around the region of interest. Our parametrization efficiency is mainly controlled by the ratio between the global search α and γ . Based on that, we arrive for our simulated case, the same correct result with a precision rate 5.2 higher. For

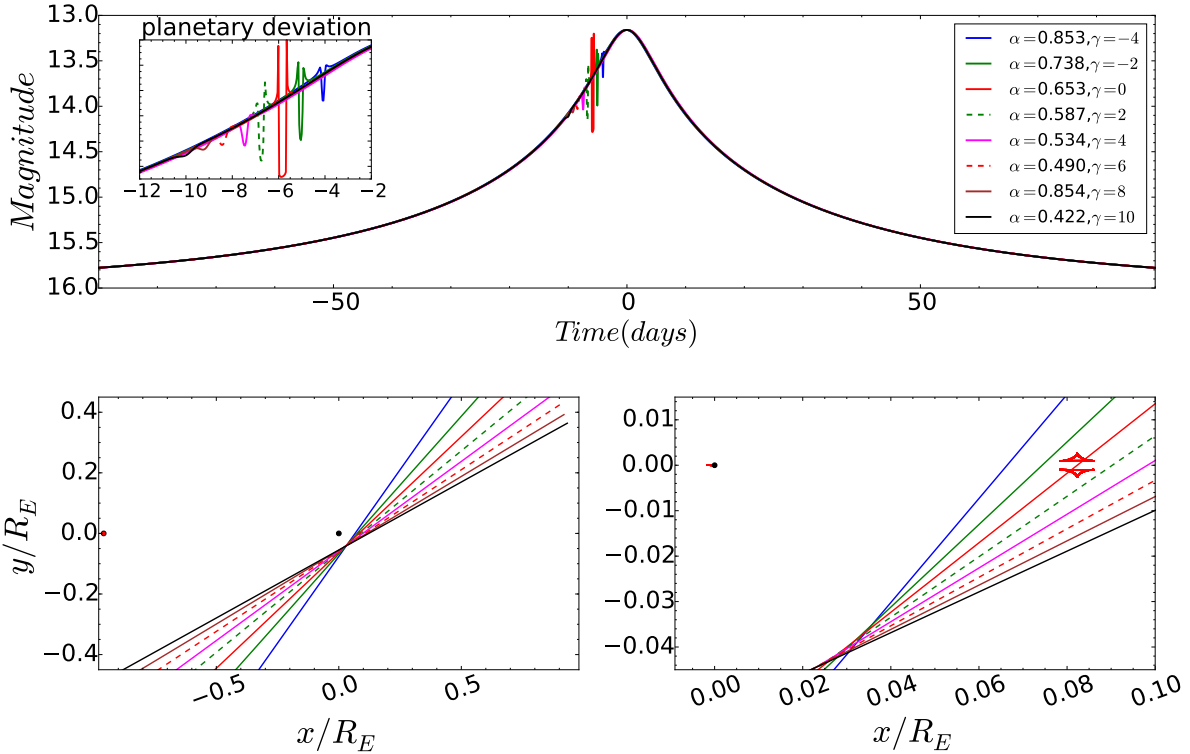


Figure 7. Top panel: 8 superposed light curves with $-4 < \gamma < 10$ for our simulated system; the planetary deviation panel shows a close-up at all the planetary signals. Bottom panels: the left panel shows the different source path for each γ on top of the topology of the system; the right panel shows the planetary caustic region in close-up.

labellightcurve3

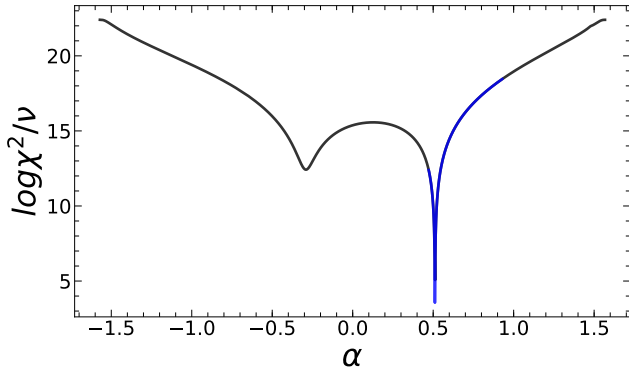


Figure 8. χ^2 diagram showing the reduced impact angle α . The blue line represents the search process by using our parametrization.

the same density of points and accuracy, our methods is 5 times faster. For a system with mass fraction and **semimajor** axis apparent similar to our Sun-Earth system and $t_E = 90$ days, we find that the planetary deviation takes about 1 day and can be observed by a **high cadence surveys**. The majority of microlensing events has typical timescale of about 20 days.

LSST with first light planned to 2019, does not plan to survey the bulge, but in any case, has cadence enough of about $1/4$ days for field events and could in principle trigger follow-up observations to search for planets. WFIRST planned to be launched in 2024 has appropriate cadence and will observe the bulge and other field.

We find that Sun-Earth analog observed system will present a close topology (for **semimajor** axis close to 1 AU) with doubled identical caustics on the other side of the planet. We also concluded that the ellipse around the planetary caustic decreases exponentially as s increases. We find that if the **semimajor** axis is equal to 1 AU, then the deviation of the light curve from the single-lens case will last for about one day (for $t_E = 90$ days). The new values for X_{ip} and Y_{ip} are implemented within the new parametrization of $\alpha(u_0)$ and can easily be integrated in the parameters search with γ dictating the evolution of α once we have defined a fixed u_0 .

We would like to thank the anonymous referee, whose important suggestions, greatly improved the paper without a doubt. We thank

to CAPES and the Federal University of Rio Grande do Norte (UFRN) for financial support.

JDNJr acknowledges financial support by Brazilian CNPq PQ 1D grant n°310078/2015-6.

REFERENCES

- Albrow, M. D., et al. 2001, Limits on the Abundance of Galactic Planets From 5 Years of PLANET Observations, *Astrophys. J. Lett.*, 556, L113
- Alcock, C., Allsman, R. A., Axelrod, T. S., et al. 1995, *Physical Review Letters*, 74, 2867
- Beaulieu, J.-P., Bennett, D. P., Kerins, E., & Penny, M. 2011, *The Astrophysics of Planetary Systems: Formation, Structure, and Dynamical Evolution*, 276, 349
- Bennett, D. P., & Rhie, S. H. 1996, *apj*, 472, 660
- Bozza, V. 2000, *aap*, 359, 1
- Cassan, A., Kubas, D., Beaulieu, J.-P., et al. 2012, *Nature*, 481, 167
- do Nascimento, J.-D., Jr., Vidotto, A. A., Petit, P., et al. 2016, *ApJL*, 820, L15
- Einstein, A. 1936, *Science*, 84, 506
- Erdl, H., & Schneider, P. 1993, *aap*, 268, 453
- Gaudi, B. S., et al. 2002, *Microensing Constraints on the Frequency of Jupiter-Mass Companions: Analysis of 5 Years of PLANET Photometry*, *Astrophys. J.*, 566, 463
- Gould, A., & Loeb, A. 1992, *apj*, 396, 104
- Gould, A., Udalski, A., Shin, I.-G., et al. 2014, *Science*, 345, 46
- Griest, K., Lehner, M. J., Cieplak, A. M., & Jain, B. 2011, *Physical Review Letters*, 107, 231101
- Han, C., Gould, A. 1995, *ApJ*, 447, 53
- Han, C. 2006, *ApJ*, 638, 1080
- Liebes, S. 1964, *Physical Review*, 133, 835
- Mao, S., & Paczynski, B. 1991, *apjl*, 374, L37
- Mayor, M., & Queloz, D. 1995, *Nature*, 378, 355
- Paczynski, B. 1986, *ApJ*, 304, 1
- Penny, M. T. 2014, *apj*, 790, 142
- Rhie, S. H. 1999, *arXiv:astro-ph/9909433*
- Rhie, S. H. et al. 2000, *On Planetary Companions to the MACHO 98-BLG-35 Microlens Star*, *Astrophys. J.*, 533, 378
- Schneider, P., & Weiss, A. 1987, *aap*, 171, 49
- Shvartzvald, Y., Yee, J.C., Calchi Novati, S., et al. 2017, *apjl*, 840
- Sumi, T., Abe, F., Bond, I. A., et al. 2003, *ApJ*, 591, 204
- Sumi, T., et al. 2006, *Microensing Optical Depth toward the Galactic Bulge Using Bright Sources from OGLE-II*, *Astrophys. J.*, 636, 240
- Udalski, A., Ryu, Y.-H., Sajadian, S., et al. 2018, *AcA*, 68, 1
- Witt H. J., 1990, *Astronomy and Astrophysics (ISSN 0004-6361)*
- Witt, J., Mao, S., 1995, *ApJ*, 447, 105
- Yee, J.C., Udalski, A., Sumi, T., et al. 2009, *apj*, 703, 2082